Ultrafast Insulator-Metal Transition in VO_2 Nanostructures Assisted by Picosecond Strain Pulses

Ia. A. Mogunov,[1,*] F. Fernández,[2] S. Lysenko,[2] A.J. Kent,[3] A.V. Scherbakov,[1,4]
A.M. Kalashnikova,[1] and A.V. Akimov[3]

[1] *Ioffe Institute, 194021 St. Petersburg, Russia*
[2] *Department of Physics, University of Puerto Rico, Mayaguez, Puerto Rico 00681, USA*
[3] *School of Physics and Astronomy, University of Nottingham, Nottingham NG7 2RD, UK*
[4] *Experimentelle Physik 2, Technische Universität Dortmund, D-44227 Dortmund, Germany*

Strain engineering is a powerful technology that exploits the stationary external or internal stress of specific spatial distribution for controlling the fundamental properties of condensed materials and nanostructures. This advanced technique modulates in space the carrier density and mobility, the optical absorption, and in strongly correlated systems, the phase, e.g., insulator-metal or ferromagnetic-paramagnetic. However, while successfully accessing nanometer-length scales, strain engineering is yet to be brought down to ultrafast time scales allowing strain-assisted control of the state of matter at THz frequencies. We demonstrate control of an optically-driven insulator-to-metal phase transition by a picosecond strain pulse, which paves the way to ultrafast strain engineering in nanostructures with phase transitions. This is realized by simultaneous excitation of VO_2 nanohillocks by a 170-fs laser and picosecond strain pulses finely timed with each other. By monitoring the transient optical reflectivity of the VO_2, we show that strain pulses, depending on the sign of the strain at the moment of optical excitation, increase or decrease the fraction of VO_2 that undergoes an ultrafast phase transition. A transient strain of moderate amplitude of approximately 0.1% applied during ultrafast photo-induced nonthermal transition changes the fraction of VO_2 in the laser-induced phase by approximately 1%. In contrast, if applied after the photoexcitation when the phase transformations of the material are governed by thermal processes, a transient strain of the same amplitude produces no measurable effect on the phase state.

I. INTRODUCTION

During the last decades, strain engineering has developed into a powerful technology to control the electron density and mobility in semiconductors. In particular, strain engineering is used for fabrication of silicon-based integrated circuits in microprocessors [1] and optical devices [2,3]. Today, the interest in emerging quantum technologies and further miniaturization of electronic and optical devices has turned strain engineering toward nano-objects such as two-dimensional layers (for reviews see Ref. [4,5]), quantum dots [6,7], and nanotubes [8]. Strain engineering utilizes stationary spatial-strain distributions for band-gap engineering [9,10], achieving high pseudo-magnetic fields [11] and anisotropic current channels [12,13]. Strain engineering has also been proposed for magnetic phase separation [14] and signal processing [15].

It is promising to extend strain engineering to the ultrafast temporal scale and control the electrons, lattice,

and spins both in space and time. It has already been shown that picosecond strain pulses can be successfully used for ultrafast modulation of internal electric fields [16], electron transport [17], laser output [18], and magnetic excitations [19–21]. In these works, the impact of picosecond strain pulses on a medium is governed by the deformation potential, piezoelectricity, or magnetostriction. However, for realistic strain amplitudes (approximately 10^{-3}), the low strength of these mechanisms means that practical applications of the technique are limited. The challenge in ultrafast strain engineering is either to develop methods to produce a much higher strain on an ultrafast time scale or to find mechanisms that provide a stronger strain-induced impact on the electronic, structural, and magnetic properties of nanostructures.

Here, we experimentally demonstrate an approach for ultrafast strain engineering, where picosecond strain pulses control ultrafast photo-induced phase transitions (PIPT) leading to radical changes in the media properties, e.g., dielectric susceptibility. The prerequisite for our work comes from the intensive studies of stationary

strain- and stress-induced effects in nano-objects fabricated from vanadium dioxide (VO_2) [22,23]. Vanadium dioxide possesses an insulator-to-metal phase transition at close-to-room temperature ($T_c = 340$ K for zero stress), and uniaxial stationary stress experiments have shown that it is a reliable material for strain nano-engineering [24,25]. The excitation of VO_2 by intense femtosecond optical pulses induces ultrafast nonthermal PIPT [26] (for review see Ref. [27]), which has also been shown to be susceptible to stationary stress or strain [28–30]. These and other studies of PIPT point to VO_2 being a prospective material for experiments where ultrafast strain engineering could be realized by combining the impacts of picosecond strain pulses and pulsed optical excitation. Our experimental studies unambiguously demonstrate that a picosecond strain pulse with an amplitude <0.1% impacts ultrafast nonthermal PIPT. A strain pulse of the same amplitude has a negligible effect on the phase transition dynamics at time scales longer than approximately 10 ps after excitation, which is governed by temperature evolution.

This article is organized as follows. In Sec. II, we describe the main structural and optical properties of the epitaxial VO_2 nanohillocks grown on an Al_2O_3 substrate, and introduce the pump-probe technique designed for combined excitation of a medium by optical and strain pulses. In Sec. III, we describe the PIPT driven in VO_2 by optical pulses and by combined action of the optical and strain pulses, as well as the effect strain pulses alone have on the VO_2. This is followed by an extended analysis presented in Sec. IV A, which shows that the strain pulses can indeed impede or enhance ultrafast PIPT in VO_2. In Sec. IV B, we discuss a phenomenological model, which qualitatively describes the impact of picosecond strain pulses on ultrafast PIPT, as well as on the nanosecond dynamics following PIPT. Conclusions and an outlook are presented in Sec. V.

II. EXPERIMENTAL

A. VO_2 nanohillocks on an Al_2O_3 substrate

The sample is a layer of epitaxial-VO_2 nanohillocks grown on a 350-μm-thick c-plane sapphire, Al_2O_3, substrate by pulsed laser deposition [31]. Atomic Force Microscope (AFM) images [Figs. 1(a) and 1(b)] show that the hillocks have a height of 70 ± 20 nm and a lateral size of 200 ± 50 nm. The VO_2 nanohillocks grown on c-cut Al_2O_3 are known to be single crystalline with the $[001]_{M1}$ axis oriented in the plane of the sapphire substrate [31–33]. Figure 1(c) shows the temperature hysteresis of the optical reflectivity R at a photon energy of 1.2 eV, and reveals the phase transition occurring at $T_c = 340$ K with a coercivity of 10 K, which is typical for thin-film and nanogranular VO_2 samples [34,35]. The changes of reflectivity from R_i to R_m at $T = T_c$ are due to the changes of the refractive

index occurring when VO_2 undergoes the transition from an insulating to a metallic phase.

The sample is prepared for the experiments with picosecond strain pulses by sputtering a 140-nm-thick Al film serving as an opto-acoustic transducer [36] on the back side of the sapphire.

B. Combined optical-and-strain pump-probe setup

Figure 1(d) shows the pump-probe experimental scheme, which allows combined excitation of a sample under study by femtosecond optical-pump and picosecond strain pulses. The laser source is a 170-fs Yb-doped $KGd(WO_4)_2$ regenerative amplifier with a central photon energy of 1.2 eV and a repetition rate of 5 kHz. Each pulse from the source is split into three pulses. The first one, shown by red in Fig. 1(d), is the optical pump pulse with a fluence W used to excite PIPT. The optical pump pulse is incident on VO_2 nanohillocks and is focused to an elliptical spot of a size of 55×100 μm^2. The second pulse, shown in blue, is used to generate the strain pulses [36] and is incident onto an Al transducer with a fluence of approximately 60 mJ/cm^2 and spot with diameter 110 μm. The third one, shown by the dashed black line in Fig. 1(d), is the probe pulse controlled by a scanning delay line and used for monitoring the temporal evolution of the reflectivity $R(t)$ from the surface with VO_2 nanohillocks. For more details, see Sec. III of the Supplemental Material [37].

We shall define the temporal reflectivity signals measured without and with strain pulses as $R_0(t)$ and $R_\varepsilon(t)$, respectively. The reflectivity $R_0(t)$ can take values between R_i and R_m, which are the stationary values of reflectivity when all nanohillocks are in the insulating or metallic phases, respectively. For the used probe photon energy of 1.2 eV (wavelength 1.03 μm), the maximum relative change of time-dependent reflectivity in our sample is $(R_m - R_i)/R_i \sim 0.1$.

III. EXPERIMENTAL RESULTS

A. Ultrafast PIPT in VO_2

Figure 1(e) demonstrates the pump-probe temporal reflectivity signal $R_0(\Delta t)$ in the absence of the strain pulse for three optical pump fluences, W, and $\Delta t = t - t_0$ (t_0 is the time when the optical pump pulse is applied). The inset in Fig. 1(e) shows the dependence of reflectivity signal R_0 on W at $\Delta t = 1$ ps after the optical pulse impact on the VO_2. In agreement with earlier works [38–42], we see that the PIPT starts to take place above the threshold $W_T = 6$ mJ/cm^2, and saturation is observed at $W > W_S = 20$ mJ/cm^2, indicating that all VO_2 nanohillocks within the probe spot have undergone PIPT under such a pump fluence [43]. The wide range of W between threshold W_T and saturation W_S results from a large dispersion of thresholds in
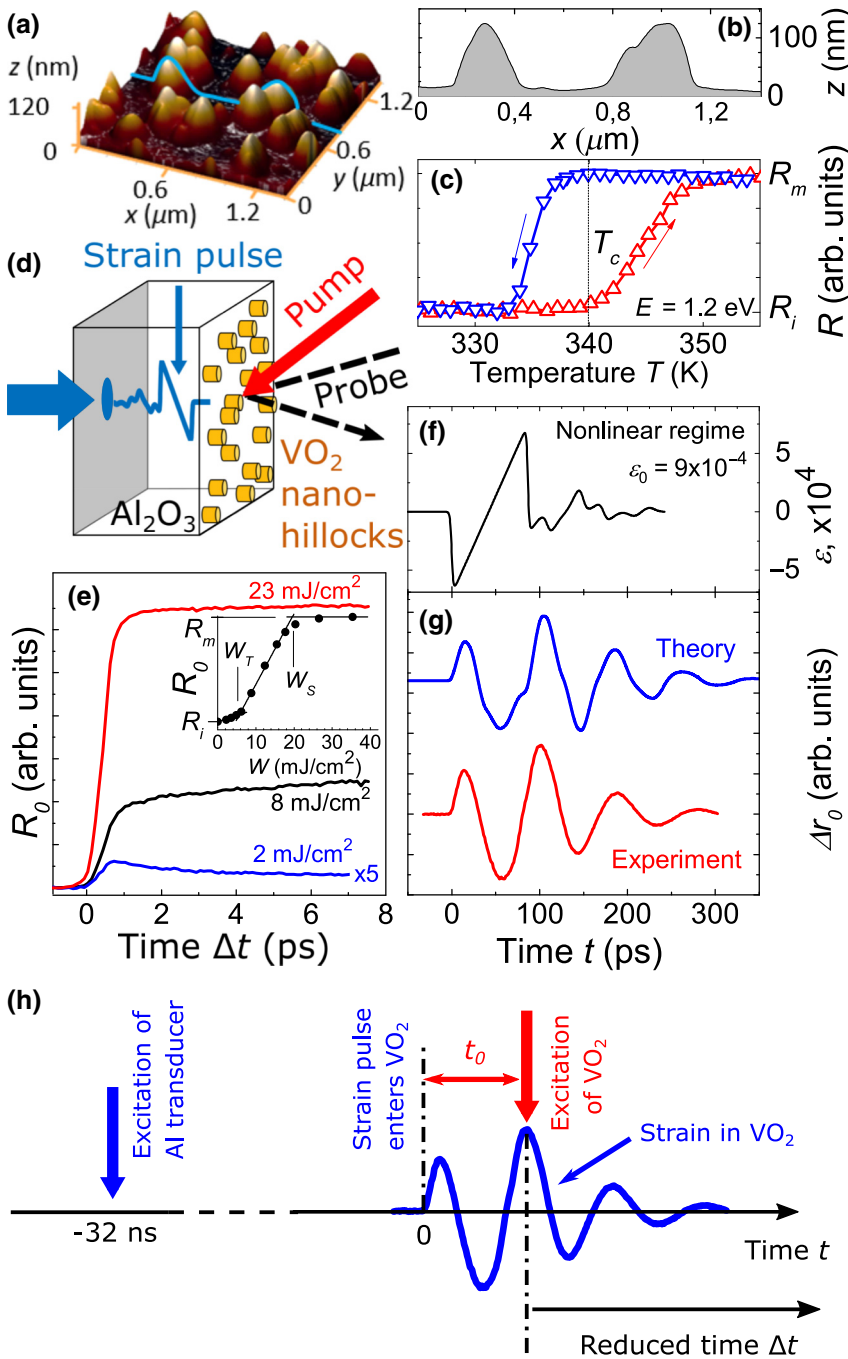
FIG. 1. Sample properties and experimental schematic. (a) AFM image of the VO₂ nanohillocks and (b) its cross section along the blue line in (a). (c) The temperature dependence of stationary reflectivity R at the photon energy 1.2 eV obtained upon heating (red symbols) and cooling (blue symbols). (d) Experimental scheme. (e) Transient reflectivity $R_0(\Delta t)$ signals obtained for three values of optical fluence W in the absence of the strain pulse. Inset shows the transient reflectivity at $\Delta t = 1$ ps as a function of W. (f) Calculated strain pulse temporal profile $\varepsilon(t)$ in nonlinear propagation regime in the sapphire substrate in the vicinity of the VO₂ nanohillocks. (g) Calculated (blue line) and measured (red line) reflective evolution of strain-induced reflectivity signal $\Delta r_0(t)$ in the absence of the optical pump ($W = 0$) corresponding to nonlinear input strain pulse shown in (f). (h) The diagram illustrating definitions of $t = 0$, $t = t_0$, and Δt, and the instants for excitations of the Al transducer and PIPT in VO₂.

the ensemble of nanohillocks with different sizes and other inhomogeneities [41]. The fraction of VO₂, which changes from an insulating to a metallic phase, may be estimated from the fluence dependence of R_0 presented in Fig. 1(e). For instance, this fraction is about 50% for the excitation density $W = 12.5$ mJ/cm².

B. Generation of strain pulses and elasto-optical response of VO₂

Following optical excitation of the Al transducer by the second pump [shown by blue in Fig. 1(d)], strain pulses are injected into the sapphire substrate and propagate through it with a sound velocity of 11 km/s, transforming into N-shaped pulses due to the nonlinear elastic properties of sapphire [44], and reach VO₂ in 32 ns. An example of the simulated temporal strain profile, $\varepsilon_0(t)$, with a strain amplitude of approximately 10^{-3} in sapphire in the vicinity of the VO₂ layer is shown in Fig. 1(f). Figure 1(g) shows the simulated and measured evolutions of strain-induced reflectivity changes $\Delta r_0(t)$ in VO₂ in the absence of the optical pump ($W = 0$). Further, we designate the strain-induced signal measured in the absence or presence of the pump beam exciting PIPT as $\Delta r_0(t)$ and

$\Delta r_W(t)$, respectively. The temporal evolution of $\Delta r_0(t)$ is governed only by the photoelastic effect in VO_2 and is proportional to the product of the mean strain $\bar{\varepsilon}(t)$ in the VO_2 nanohillocks and the photoelastic constant p (p_i or p_m in the insulating and metallic phases, respectively). The signal $\Delta r_0(t)$ exhibits oscillatory behavior, and the temporal intervals where the signal is positive and negative correspond to out-of-plane compression and tension, respectively. The details of the strain and reflectivity simulations may be found in Sec. I of Supplemental Material [37]. The optical parameters of VO_2 are taken from [45].

C. Ultrafast PIPT in VO_2 under combined excitation by optical and strain pulses

To examine the effect of a strain pulse on PIPT, we study the reflectivity changes $\Delta r_W(t)$ of the VO_2 nanohillocks under simultaneous impact of both strain and optical pump pulses. The diagram in Fig. 1(h) shows the sequence of incident optical pulses and strain pulse on the sample. The delay t_0 is the time interval between the moments when the front edge of the strain pulse enters VO_2 and the optical pump pulse triggers PIPT. The value of t_0 is set to a specific value during the experiments. By changing the delay t_0, we induce PIPT during the strain pulse present in VO_2 (i.e., $t_0 > 0$) or before the strain pulse reaches the interface between sapphire and nanohillocks (i.e., $t_0 < 0$). Since the duration of the strain pulse when it reaches VO_2 is approximately 100 ps [Fig. 1(f)], we can precisely adjust the temporal delay t_0 of the 170-fs optical pump in such a way that the latter excites the VO_2 nanohillocks during the action of out-of-plane compressive or tensile strain $\bar{\varepsilon}(t)$. The reflectivity changes are probed at a variable time t, which is counted from the moment the front edge of the strain pulse enters the VO_2 ($t = 0$).

The detection in our experiment is realized in a way that only the strain-induced changes of the reflectivity are monitored, either with or without the impact of the optical pump inducing PIPT, i.e., $\Delta r_0(t)$ or $\Delta r_W(t)$, respectively (for details see [37]). Then in the case of simultaneous excitation of VO_2 nanohillocks by optical pump and strain pulse, the strain-induced probe signal $\Delta r_W(t)$ may be written as:

$$\Delta r_W(t) = p(t)\bar{\varepsilon}(t) + [R_\varepsilon(t, t_0) - R_0(t - t_0)] \quad (1)$$

Here, the first term describes the photoelastic response proportional to the strain $\bar{\varepsilon}(t)$ in VO_2 and $p(t)$ is a corresponding photoelastic constant. Both $\bar{\varepsilon}(t)$ and $p(t)$ depend on the phase, insulating or metallic, of VO_2, and thus for $W \neq 0$, the photoelastic constant is a time-dependent function and depends on W and t_0. Only in the case of $W = 0$ we get $\Delta r_W(t) = \Delta r_0(t) = p_i\bar{\varepsilon}(t)$, where p_i is a photoelastic constant in the insulator phase. The second

term in Eq. (1), which is the difference of the reflectivities with and without strain pulse [$R_\varepsilon(t, t_0)$ and $R_0(t - t_0)$, respectively], corresponds to the changes in the reflectivity governed by the changes in refractive index due to PIPT [for $R_0(t - t_0)$ see Fig. 1(e)]. $R_\varepsilon(t, t_0)$ and $R_0(t - t_0)$ have values between R_i and R_m and provide information on the VO_2 fraction transformed into the metallic phase. The main goal of the experiments is to find the difference $\Delta R_\varepsilon(t, t_0) = R_\varepsilon(t, t_0) - R_0(t - t_0)$ associated with the strain-induced changes of a fraction that has experienced PIPT.

We obtain $\Delta R_\varepsilon(t, t_0)$ by subtracting the photoelastic contribution $p(t)\bar{\varepsilon}(t)$ in Eq. (1) from the measured $\Delta r_W(t)$. For this, we start with the case when optical excitation W exceeds the saturation level, W_S, and all VO_2 hillocks undergo PIPT to the metallic phase. The effect of the strain pulse on the PIPT in this case should be negligible, which means that $\Delta R_\varepsilon(t, t_0) = 0$, and all changes in $\Delta r_W(t)$ are due only to the photoelastic effect. The results are presented in Fig. 2(a). The main, red, curve represents the measured signal when the optical pulse excites VO_2 simultaneously with the strain pulse at a delay of
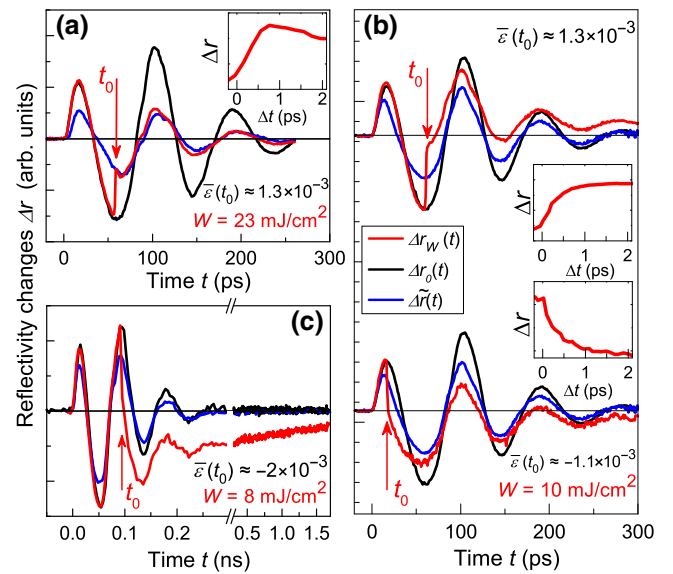

FIG. 2. Temporal evolutions of the reflectivity changes in the VO_2 nanohillocks under the impact of the picosecond strain pulse measured in the time intervals 300 ps (a, b) and 1700 ps (c). Black and red curves are the signals measured without [$\Delta r_0(t)$] and with [$\Delta r_W(t)$] optical pump, respectively. Vertical arrows indicate the time $t_0 > 0$ when the optical pump is applied. Blue lines correspond to $\Delta \tilde{r}(t)$ when the optical pulse excites the VO_2 nanohillocks before the arrival of the strain pulse, $t_0 = -30$ ps. In (b) and (c), the optical pump densities W are above the threshold, $W > W_T$, and below the saturation level, $W < W_S$, for PIPT; in (a) $W > W_S$. The insets in (a) and (b) show $\Delta r(t)$ vs reduced time $\Delta t = t - t_0$ measured around t_0 with a temporal resolution of 200 fs. Also indicated are the mean strain amplitudes $\bar{\varepsilon}$ at the moment of the photoexitation t_0 (see for details Sec. I and Fig. S5 in Supplementary Material [37]).

$t_0 = 60$ ps, corresponding to the tensile part of the out-of-plane component of the strain pulse. A sudden change takes place in $\Delta r_W(t)$ at $t = t_0$ [for highly resolved temporal evolution see the inset in Fig. 2(a)]. The black curve corresponds to a signal $\Delta r_W(t) = \Delta r_0(t) = p_i \bar{\varepsilon}(t)$ at $W = 0$, when all nanohillocks are in the insulating phase [see also Fig. 1(g)]. The blue curve is the signal $\Delta \tilde{r}(t) = \Delta r_W(t)|_{t_0 < 0}$ obtained when the optical pulse hits the VO₂ before the arrival of the strain pulse. We show that for $W > W_S$, $\Delta \tilde{r}(t)$ is equal to $\Delta r_m(t) = p_m \bar{\varepsilon}(t)$ (p_m is the photoelastic constant in the metallic phase), which is a reflectivity change when all VO₂ nanohillocks are in the metallic phase (see Sec. II in Supplemental Material [37]). It is seen in Fig. 2(a) that at $t = t_0 = 60$ ps [see red curve in Fig. 2(a)], $\Delta r_W(t)$ switches abruptly from the photoelastic response in the insulator phase [$\Delta r_W(t) = \Delta r_0(t)$ at $t < t_0$] to the response in the metallic phase [$\Delta r_W(t) = \Delta r_m(t)$ at $t > t_0$]. Two important conclusions can be drawn from this result. First, transient signals $\Delta r_W(t) = \Delta r_0(t)$ at all times $t < t_0$, confirming that VO₂ nanohillocks are in the insulator phase before the impact of the optical pump. Second, transient signals $\Delta r_W(t) = \Delta \tilde{r}(t) \equiv \Delta r_m(t)$ at $t > t_0$. The transient around $t = t_0$ shown in the inset of Fig. 2(a) lasts less than 1 ps. Since $\Delta R_\varepsilon(t, t_0) = 0$ for $W > W_S$, the effect of abrupt change of $\Delta r_W(t)$ at $t = t_0$ can be ascribed with confidence to the changes of the photoelastic constant p upon the transition from an insulating to a metallic phase.

The case shown in Fig. 2(a) gives us a recipe for extracting $\Delta R_\varepsilon(t, t_0)$ for any W, which is the main goal of the experiment. This is done by comparing triads of signals $\Delta r_W(t)$, $\Delta r_0(t)$, and $\Delta \tilde{r}(t)$ measured for the same $W_T < W < W_S$ (for details see Sec. II in Supplemental Material [37]):

$$\Delta R_\varepsilon(t, t_0) = \begin{cases} \Delta r_W(t) - \Delta r_0(t) = 0, & t < t_0, \\ \Delta r_W(t) - \Delta \tilde{r}(t), & t > t_0. \end{cases} \quad (2)$$

Now we turn to the most important part of the experiment, where we measure $\Delta r_W(t)$ for intermediate optical fluences $W_T < W < W_S$ when a certain fraction of VO₂ nanohillocks undergoes PIPT. Figures 2(b) and 2(c) show corresponding triads: signals $\Delta r_W(t)$ with simultaneous excitation of PIPT and strain pulse (red curves); signals $\Delta r_0(t)$ for $W = 0$ (black curves); and signals $\Delta \tilde{r}(t)$ measured when $t_0 < 0$ (blue curves). Again, the subpicosecond changes in transient reflectivity $\Delta r_W(t)$ take place at $t = t_0$ [see insets in Fig. 2(b)]. However, in strong contrast to data obtained at $W > W_S$ [Fig. 2(a)], at $t > t_0$, the transient reflectivity $\Delta r_W(t)$ clearly differs from $\Delta \tilde{r}(t)$, and thus $\Delta R_\varepsilon(t, t_0) \neq 0$ according to Eq. (2) after the pump pulse (i.e., at $t > t_0$). The signals $\Delta r_W(t)$ at $t > t_0$ are characterized not only by the reduced amplitude of oscillations, but these oscillations are superimposed on a different baseline. The latter effect is most evident at a nanosecond time scale [Fig. 2(c)], when the monotonously decaying behavior of $\Delta r_W(t)$ is clearly

seen. At long time delays $t > 300$ ps, when $\bar{\varepsilon}(t) = 0$ in the VO₂ nanohillocks, the photoelastic contribution in $\Delta r_W(t)$ [Eq. (1)] vanishes, leaving only the nonzero contribution $\Delta R(t, t_0)$, which is related to strain-induced changes of the fraction of VO₂ which undergoes PIPT.

It is important that this slow decaying transient reflectivity $\Delta r_W(t)$ and, consequently, the nonzero $\Delta R_\varepsilon(t, t_0)$, is observed only for optical pump densities W between the PIPT threshold W_T and saturation values W_S. Furthermore, at elevated temperature $T = 360$ K when all VO₂ is initially in the metallic phase, no abrupt changes in $\Delta r_W(t)$ are detected at any W and t_0 (see Sec. IV in Supplemental Material [37]).

IV. DISCUSSION

A. Impact of the strain on ultrafast and nanosecond PIPT

The main experimental result of the present work is the observation of strain-induced subpicosecond changes of the optical reflectivity associated with PIPT. These changes, defined in our work as $\Delta R_\varepsilon(t, t_0)$, are beyond the photoelastic effect, whose contribution may be subtracted from the measured signal $\Delta r_W(t)$ using the procedure described above [see also Figs. 3(a) and 3(b)]. We attribute $\Delta R_\varepsilon(t, t_0)$ to the strain-induced changes in the fraction of VO₂ nanohillocks undergoing insulator-metal phase transition during PIPT. The main argument in favor of this statement is the observation of a long nanosecond decay of $\Delta R_\varepsilon(t, t_0)$ when the strain pulse in VO₂ is gone and there is no contribution from the photoelastic effect. The analysis of the transients $\Delta R_\varepsilon(t, t_0)$ obtained for different delays t_0 and different optical pump fluencies W leads us to the following conclusions:

(i) Strain-induced decrease (increase) of the proportion of VO₂ nanohillocks undergoing PIPT takes place when out-of-plane compression (tension) takes place. In the experiments with strain pulses, it is possible to control the sign and value of strain by precisely choosing the moment t_0 of optical impact inducing PIPT;

(ii) Only at the moment of the optical pulse impact do the magnitude and sign of the strain $\bar{\varepsilon}(t_0)$ define the strength of the strain-induced effect on PIPT and the related quantitative difference $\Delta R_\varepsilon(t, t_0)$.

Conclusion (ii) means that the role of strain in PIPT is important only during ultrafast transients, which include complex electron and lattice transformations and the presence of intermediate phases with subpicosecond lifetimes (for review see Ref. [27]). Although our experiments do not allow us to distinguish whether strain mostly affects the electron or phonon systems, it is clear that strain does not have any effect on the state present on the longer time scales when recovery to the insulator phase is accompanied

by thermal processes and sometimes metastable states with nanosecond transient times [42,46]. It is important to stress that it is not possible to make conclusion (ii) based on the experiments with the stationary strain [30].

To further support statements (i) and (ii), we plot in Fig. 3(c) transients $\Delta R_\varepsilon(t, t_0)$ vs the reduced time $\Delta t = t - t_0$ at $W = 9$ mJ/cm^2 and at two values of $t_0 = 60$ ps and 95 ps, corresponding to maximum of out-of-plane compression and tension, respectively. It is seen that there are two contributions to the decay of $\Delta R_\varepsilon(\Delta t)$ for both t_0 values: fast and slow, with respective amplitudes A_F and A_S. The slow decay with time constant >1 ns is the relaxation of the material to the quasi-equilibrium state following PIPT, which lasts for microseconds, and most likely is governed by the local temperature equilibration in the excited spot [47]. The slow decay is not observed when PIPT is induced at t_0 close to the moment when $\Delta r_0(t)$ changes sign (see Sec. II in Supplemental Material [37]). These observations are consistent with the fact that the strain pulse does not change the temperature of the VO$_2$ and thus does not affect the processes underlying relaxation of the material to the quasi-equilibrium state at which $\Delta R_\varepsilon = 0$.

Figures 3(d) and 3(e) show the optical pump fluence W dependencies of A_S and A_F obtained as shown in

Fig. 3(c). The results for A_S confirm our main conclusions (i) and (ii). $A_S \approx 0$ when $W < W_T$, and is also zero when W exceeds the saturation level. From comparison of the measured relative changes of the extracted $\Delta R_\varepsilon/R_i \sim 10^{-4}$ (R_i is the stationary reflectivity in the insulator phase) and signal $\Delta R_0/R_i \sim 10^{-2}$ measured in the absence of the strain pulse, we estimate the maximum additional fraction of VO$_2$ nanohillocks under input strain to be approximately 1% from the nanohillocks, which undergo PIPT at $W = 9$ mJ/cm^2. This estimate is correct only to the order of magnitude because it is made under the assumption of linear proportionality between the studied layer's effective dielectric permittivity and the fraction of material of nanohillocks in the metallic state. One can also expect a shift of the excitation threshold for PIPT under the strain pulse excitation. However, it is known from experiments with stationary stress [30] that the 5-GPa stress is required to decrease the threshold W_T to 0. In our experiments, the maximum stress in the picosecond strain pulse is 0.1 GPa and then we may expect a threshold shift of about 1%, which agrees well with the maximum observed strain-induced change of PIPT. Such a shift of W_T cannot be clearly detected due to the fact that the onset of PIPT at W_T is smeared due to inhomogeneity of the nanohillocks' sizes, internal stresses, etc.
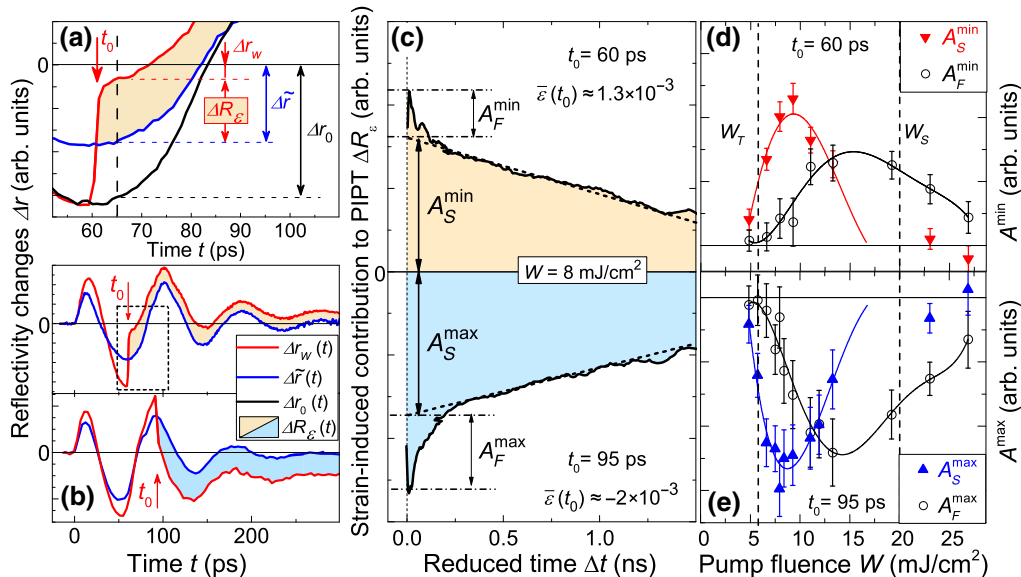

FIG. 3.   Strain-induced effect in the ultrafast phase transition. (a) Illustration of the procedure [Eq. (2)] for extracting the contribution $\Delta R_\varepsilon(t, t_0)$ due to strain present during the photoexcitation (at $t_0 = 60$ ps) from the total signal $\Delta r_w(t)$ measured at $t = 65$ ps. The black and red curves are the signals measured without [$\Delta r_0(t)$] and with [$\Delta r_W(t)$] optical pump. Vertical arrows indicate the time $t_0 = 60$ ps when the optical pump is applied. Blue lines correspond to $\Delta r(t)$ when the optical pulse excites the VO$_2$ nanohillocks before the arrival of the strain pulse, $t_0 = -30$ ps [see also Fig. 2(b)]. (b) Expanded view of frame (a) for $t_0 = 60$ ps (upper panel) and $t_0 = 95$ ps (lower panel) in the time interval of 300 ps. Shaded areas show $\Delta R_\varepsilon(t, t_0)$ and highlight that the sign of this strain-induced contribution is conserved over the whole temporal range $t > t_0$. (c) Temporal evolutions of the extracted contribution $\Delta R_\varepsilon(t)$ to the PIPT induced by out-of-plane tensile [$\bar\varepsilon(t_0 = 60$ ps$) \approx 1.3 \times 10^{-3}$, upper] and compressive [$\bar\varepsilon(t_0 = 95$ ps$) \approx -2 \times 10^{-3}$, lower] strain. (d,e) Optical pump fluence dependences of the amplitudes of the fast A_F (open circles) and slow A_S (closed triangles) components of $\Delta R_\varepsilon(t)$ as obtained for out-of-plane tensile (d) and compressive (e) strain. Solid lines are guides to the eye. Vertical dashed lines mark the PIPT threshold W_T and saturation W_S optical pump fluencies.

The contribution A_F of the fast-decaying component in $\Delta R_\varepsilon(\Delta t, t_0)$ is negligible at $W < 6$ mJ/cm^2, but it increases rapidly at higher W and vanishes only at $W > 26$ mJ/cm^2, which essentially exceeds W_S. A nonzero contribution from the fast-decaying $\Delta R_\varepsilon(\Delta t, t_0)$ is also observed when PIPT is excited at t_0 close to the moment when $\Delta r_0(t)$ changes sign, and no slow contribution, attributed to the change of the VO$_2$ fraction undergoing PIPT, is present (see Sec. II in Supplemental Material [37]). The origin of such behavior most likely is partly due to the difference of the elastic parameters of VO$_2$ in the insulator and metallic phases resulting in the dependence of $\bar{\varepsilon}(t)$ on the VO$_2$ phase [48]. It can also be related to the complex kinetics of the phase transition in the time interval $t = 1$–100 ps [42,46], for instance, to the strain-induced changes of photoexcited carriers' density reported in [28].

B. Mechanism for strain-induced changes of ultrafast PIPT

The results described above unambiguously suggest that strain corresponding to out-of-plane compression (tension) applied at the moment of the optical pump impact impedes (supports) the subpicosecond insulator-to-metal transition and switching of the crystalline lattice to a new symmetry state (for VO$_2$ from a monoclinic to a rutile lattice cell) during PIPT. It is important that the impact of strain on the fraction of the VO$_2$ undergoing PIPT is observed only during a time less than 1 ps after the femtosecond optical-pump pulse. A strain of the same amplitude acting on the VO$_2$ nanohillocks before, or at $t > 1$ ps after, the laser-pulse impact does not have any effect on PIPT [43].

To explain these findings on a qualitative level, we employ the phenomenological model of the first-order structural PIPT in a single domain of VO$_2$ [42,49,50] and extend it to the case of combined laser- and strain-pulse impacts. In this model, the thermodynamic potential Φ is introduced as a Landau expansion of the free energy [51] for the order parameter η:

$$\Phi(\eta) = \frac{\alpha(W,\varepsilon)}{2}\eta^2 + \frac{\beta}{4}\eta^4 + \frac{\gamma}{6}\eta^6, \qquad (3)$$

where the parameter $\alpha(W,\varepsilon) > 0$ is dependent on the exciting optical-pump fluence and the applied strain, and $\beta < 0$ and $\gamma > 0$ are constants independent of W and ε, the values of which were found experimentally in [42]. Here, the order parameter η is the generalized lattice distortion associated with lattice transformation from a monoclinic to a rutile phase, and $\Phi(\eta)$ is the energy of the system of two V atoms.

The present model considers the single-domain nanoparticle and serves as a valid approximation for an individual nanohillock, which most likely either transits to a metallic phase or not as a whole [52]. However, if the size of a nanohillock allows the coexistence of two phases within it, then Eq. (3) should be expanded with a term accounting for an energy penalty resulting from the emergence of the interphase boundary.

The thermodynamic potential $\Phi(\eta)$ for VO$_2$ in the equilibrium insulating monoclinic phase is shown in Fig. 4 by a solid black line labeled as "Ground state". The value of η_C corresponds to the equilibrium position of atoms in the insulating monoclinic phase and equals to the root-mean-square displacement of all atoms of VO$_2$ during the transition. Excitation by a femtosecond laser pulse drives the system into a nonequilibrium excited state, which is characterized by the presence of two minima in $\Phi(\eta)$. These minima correspond to the laser-induced rutile phase at $\eta = 0$, and the metastable monoclinic phase at $0 < \eta < \eta_C$ [42]. The black line "Excited state" in Fig 4(a) shows an example of $\Phi(\eta)$ for photoexcited VO$_2$ in the case of moderate optical-pump fluence $W_T < W < W_S$. Excitation of the nonequilibrium state triggers the structural phase transition, which proceeds in two steps [42,43]: At the initial stage, the laser-pulse fluence $W_T < W < W_S$ is sufficient for an over-barrier excitation and yields partial transitions to both minima corresponding to the rutile and metastable monoclinic phases. The fraction of VO$_2$ in the rutile phase after excitation is determined by the height of the barrier ΔG [see inset in Fig. 4(a)]. This initial stage for structural PIPT is governed by coherent optical phonons and develops at a time $\tau_1 \lesssim 1$ ps [42,43]. After that, the system appears either in the rutile phase or in a potential well of the metastable monoclinic state at $0 < \eta < \eta_C$. The second stage includes slow ($\tau_2 > 1$ ns) thermally activated transitions over the barrier ΔG from the metastable monoclinic to a rutile phase and a final cooling approaching the equilibrium monoclinic phase.

The applied strain changes the parameter $\alpha(W,\varepsilon)$ in the thermodynamic potential $\Phi(\eta)$ of the photoexcited system, given by Eq. (3) [see red and blue lines in Fig. 4(a)] [53]. Since PIPT is complete at this time scale, which is significantly shorter than the characteristic time of strain modulation in our pulse, the system during PIPT is affected by the strain as if it was a quasistationary one, with a particular magnitude and sign. Therefore, the strain increases or decreases the over-barrier excitation energy [see vertical arrows in Fig. 4(a)], and thus alters the fraction of VO$_2$ in the rutile phase at the first (i.e., picosecond) stage of PIPT, as indicated by the symbols in Fig. 4(a). Such a model explains, on a qualitative level, the experimentally observed strain-induced effect on PIPT during $t \sim \tau_1$ following optical excitation.

The second (i.e., nanosecond) stage of PIPT should also be sensitive to the strain due to the strain modulation of the barrier height ΔG [see inset in Fig. 4(a)]. However, in contrast to the impact of strain at the first ultrafast
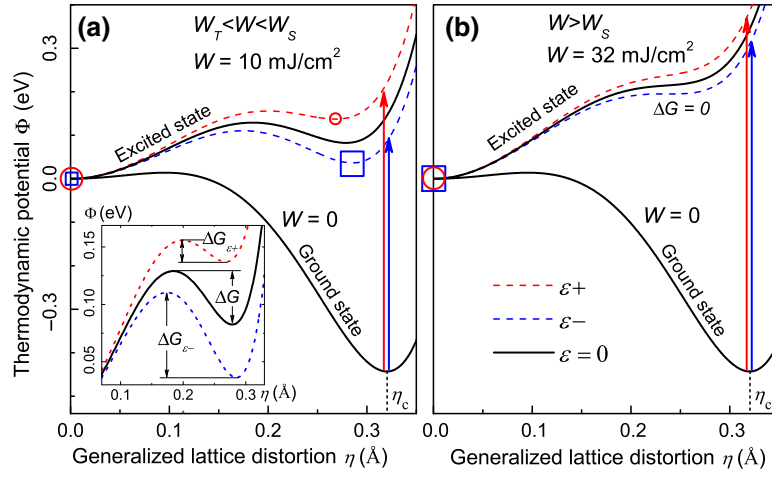
FIG. 4.   Thermodynamic potentials $\Phi(\eta)$ [Eq. (3)] in the initial monoclinic phase (solid lines) and after the photoexcitation (dashed lines) by a femtosecond pulse of intermediate fluence (a) and in the saturation regime (b), calculated using the parameters determined in [42]. Black lines show the thermodynamic potential of the unstrained system. Red and blue lines are the potentials corresponding to the strain components, which increase ($\varepsilon+$) or decrease ($\varepsilon-$) the free energy of the photoexcited system, respectively. Note that the distortion of $\Phi(\eta)$ due to strain is exaggerated for the sake of clarity. Vertical arrows show the photoexcitation process in the sample in the presence of strain. Symbols and their sizes schematically indicate a probability for the system to occur in the rutile ($\eta = 0$) or metastable monoclinic ($0 < \eta < \eta_C$) state after approximately 1 ps following the photoexcitation of the sample subjected to the strain-induced increase (red circles) or decrease (blue squares) of $\Phi(\eta)$ at $\eta = \eta_C$. Inset shows the strain-induced change of the potential barrier ΔG between the photoexcited rutile and metastable monoclinic states.

stage of PIPT, the slow over-barrier transition can be efficiently modulated by strain only if the latter is applied during time $t \gtrsim \tau_2$. It is easy to show that the amplitude of the strain-induced modulation of the rutile phase at this stage is proportional to $(\omega\tau_2)^{-1}$, where ω is a characteristic radial frequency of the coherent acoustic phonon wave packet in the strain pulse. In our experiments, $\omega \sim 10^{11}$ rad·s^{-1} and $(\omega\tau_2)^{-1} \leq 10^{-2}$, which means that modulation by strain is two orders of magnitude more efficient at the first ultrafast stage of PIPT than at the second nanosecond stage when over-barrier processes are required for structural phase transition. This accounts for the absence of the strain-induced modulation on the PIPT at time scales longer that 1 ps after the optical excitation [Fig. 3(c)].

In the saturation regime, when the laser pulse fluence $W > W_S$, the minimum in $\Phi(\eta)$ corresponding to the metastable monoclinic phase vanishes, and the complete PIPT to the rutile phase occurs at the first ultrafast stage of PIPT [Fig. 4(b)]. In this case, a moderate strain applied to VO$_2$ is not sufficient to introduce the second minimum in $\Phi(\eta)$ at $0 < \eta < \eta_C$, and thus PIPT is insensitive to the impact of strain pulses. This is consistent with our experimental observations.

Finally, we note that the symmetry of the VO$_2$ nanohillocks used in the experiments requires in-plane strain components [22,23] to influence the lattice switching. The injected strain components ε_{zz} (z is a direction perpendicular to the surface plane) are out-of-plane, but in-plane components are generated in the

VO$_2$ hillocks if their diameters are not much larger than their heights [54,55]. This is indeed the case for the studied VO$_2$ nanohillocks, which have a diameter-to-height ratio of approximately 3 [Fig. 1(a)]. Thus, we argue that in our experiments, the tensile (compressive) in-plane strain reduces (increases) the fraction of VO$_2$ undergoing PIPT, which is in agreement with the static experiments [22,23].

V. CONCLUSIONS

We show that the impact of picosecond strain pulses with amplitudes of approximately 10^{-3} decreases or increases, depending on the sign of strain, the fraction of VO$_2$ nanohillocks that undergo ultrafast PIPT from an insulating to a metallic phase. This impact occurs only at a subpicosecond time range after optical pulse excitation. After the strain pulse, the relaxation of the excess or deficient fraction of VO$_2$ in the metallic phase to quasi-equilibrium takes place in a nanosecond time scale, which is faster than for the full recovery of VO$_2$ from PIPT.

The observed approximately 1% change of strain-induced modulation of the VO$_2$ volume undergoing the phase transition may be significantly enhanced by increasing the picosecond strain amplitude from 0.1% up to state-of-the-art values of approximately 1.5% [56,57]. Furthermore, in a single-domain nanoobject, e.g., a single nanohillock, the excitation threshold for PIPT will be well defined and not spread over the wide range of optical intensities. In this case, the compressive and tensile components

of the picosecond strain pulse should notably increase or decrease the threshold value for PIPT. In such a system of well-defined nanoelements, the picosecond-strain-assisted enhancement or suppression of the ultrafast PIPT may lead to prospective applications in CMOS and photonic technologies [58–61]. Since dynamical strain may be localized down to a nanometer scale [62], it can be used as a tool for selective control of single VO$_2$ nanoelements. One can envisage an all-optically controlled nanoarray of ultrafast electrical and/or optical switches, where the optical excitation selectively drives the transition to the metallic state in an element of the array, which is subject to dynamical strain at the moment of excitation.

The demonstrated effect is not limited to the particular material and type of phase transitions studied here. The feasibility of the control of PIPT in VO$_2$ by picosecond strain pulses paves the way to ultrafast strain engineering in materials with magnetic phase transitions where femtosecond photo-induced changes of magnetic state have been revealed [63–66]. Ultrafast strain engineering may also facilitate yet-to-be-demonstrated laser-driven control of ferroelectricity in complex structures, i.e., heterostructures and patterned nanolayers, which include optically opaque and transparent materials possessing phase transitions. Picosecond strain pulses may be generated selectively in space, thus allowing control of strain-induced effects on both nanometer and picosecond scales in space and time, respectively.

ACKNOWLEDGMENTS

[1] P. R. Chidambaram, C. Bowen, S. Chakravarthi, C. Machala, and R. Wise, Fundamentals of silicon material properties for successful exploitation of strain engineering in modern CMOS manufacturing, IEEE Trans. Electron Devices **53**, 944 (2006).

[2] R. S. Jacobsen, K. N. Andersen, P. I. Borel, J. Fage-Pedersen, L. H. Frandsen, O. Hansen, M. Kristensen, A. V. Lavrinenko, G. Moulin, H. Ou, C. Peucheret, B. Zsigri, and A. Bjarklev, Strained silicon as a new electro-optic material, Nature **441**, 199 (2005).

[3] J. Michel, J. F. Liu, and L. C. Kimerling, High-performance Ge-on-Si photodetectors, Nat. Photon **4**, 527 (2010).

[4] R. Roldán, A. Castellanos-Gomez, E. Cappelluti, and F. Guinea, Strain engineering in semiconducting two-dimensional crystals, J. Phys.: Condens. Matter. **27**, 313201 (2015).

[5] C. Si, Z. Sun, and F. Liu, Strain engineering of graphene: A review, Nanoscale **8**, 3207 (2016).

[6] F. Guffarth, R. Heitz, A. Schliwa, O. Stier, N. N. Ledentsov, A. R. Kovsh, V. M. Ustinov, and D. Bimberg, Strain engineering of self-organized InAs quantum dots, Phys. Rev. B **64**, 085305 (2001).

[7] Y. Zhang, Y. Chen, M. Mietschke, L. Zhang, F. Yuan, S. Abel, R. Hühne, K. Nielsch, J. Fompeyrine, F. Ding, and O. G. Schmidt, Monolithically integrated microelectromechanical systems for on-chip strain engineering of quantum dots, Nano Lett. **16**, 5785 (2016).

[8] H. M. Ghassemi, C. H. Lee, Y. K. Yap, and R. S. Yassar, Field emission and strain engineering of electronic properties in boron nitride nanotubes, Nanotechnology **23**, 105702 (2012).

[9] H. J. Conley, B. Wang, J. I. Ziegler, R. F. Haglund, Jr., S. T. Pantelides, and K. I. Bolotin, Bandgap engineering of strained monolayer and bilayer MoS$_2$, Nano Lett. **13**, 3626 (2013).

[10] F. Guinea, M. I. Katsnelson, and A. K. Geim, Energy gaps and a zero-field quantum Hall effect in graphene by strain engineering, Nat. Phys. **6**, 30 (2010).

[11] N. Levy, S. A. Burke, K. L. Meaker, M. Panlasigui, A. Zettl, F. Guinea, A. H. Castro Neto, and M. F. Crommie, Strain-induced pseudo–magnetic fields greater than 300 Tesla in graphene nanobubbles, Science **329**, 544 (2010).

[12] V. M. Pereira and A. H. C. Neto, Strain Engineering of Graphene's Electronic Structure, Phys. Rev. Lett. **103**, 046801 (2009).

[13] R. Fei and L. Yang, Strain-engineering the anisotropic electrical conductance of few layer black phosphorus, Nano Lett. **14**, 2884 (2014).

[14] K. Lai, M. Nakamura, W. Kundhikanjana, M. Kawasaki, Y. Tokura, M. A. Kelly, and Z.-X. Shen, Mesoscopic percolating resistance network in a strained manganite thin film, Science **329**, 190 (2010).

[15] K. Roy, S. Bandyopadhyay, and J. Atulasimha, Hybrid spintronics and straintronics: A magnetic technology for ultra low energy computing and signal processing, Appl. Phys. Lett. **99**, 063108 (2011).

[16] M. R. Armstrong, E. J. Reed, K.-Y. Kim, J. H. Glownia, W. M. Howard, E. L. Piner, and J. C. Roberts, Observation of terahertz radiation coherently generated by acoustic waves, Nat. Phys. **5**, 285 (2009).

[17] D. M. Moss, A. V. Akimov, B. A. Glavin, M. Henini, and A. J. Kent, Ultrafast Strain-Induced Current in a GaAs Schottky Diode, Phys. Rev. Lett. **106**, 066602 (2011).

[18] C. Brüggemann, A. V. Akimov, A. V. Scherbakov, M. Bombeck, C. Schneider, S. Hofling, A. Forchel, D. R. Yakovlev, and M. Bayer, Laser mode feeding by shaking

quantum dots in a planar microcavity, Nat. Photon **6**, 30 (2012).

[19] A. V. Scherbakov, A. S. Salasyuk, A. V. Akimov, X. Liu, M. Bombeck, C. Brüggemann, D. R. Yakovlev, V. F. Sapega, J. K. Furdyna, and M. Bayer, Coherent Magnetization Precession in Ferromagnetic (Ga, Mn)As Induced by Picosecond Acoustic Pulses, Phys. Rev. Lett. **105**, 117204 (2010).

[20] J.-W. Kim, M. Vomir, and J.-Y. Bigot, Ultrafast Magnetoacoustics in Nickel Films, Phys. Rev. Lett. **109**, 166601 (2012).

[21] D. Afanasiev, I. Razdolski, K M Skibinsky, D. Bolotin, S V Yagupov, M B Strugatsky, A. Kirilyuk, Th. Rasing, and A V Kimel, Laser Excitation of Lattice-Driven Anharmonic Magnetization Dynamics in Dielectric $FeBO_3$, Phys. Rev. Lett. **112**, 147403 (2014).

[22] J. H. Park, J. M. Coy, T. S. Kasirga, C. Huang, Z. Fei, S. Hunter, and D. H. Cobden, Measurement of a solid-state triple point at the metal–insulator transition in VO_2, Nature **500**, 431 (2013).

[23] Y. Chen, S. Zhang, F. Ke, C. Ko, S. Lee, K. Liu, B. Chen, J. W. Ager, R. Jeanloz, V. Eyert, and J. Wu, Pressure−temperature phase diagram of vanadium dioxide, Nano Lett. **17**, 2512 (2017).

[24] J. Cao, E. Ertekin, V. Srinivasan, W. Fan, S. Huang, H. Zheng, J. W. L. Yim, D. R. Khanal, D. F. Ogletree, J. C. Grossman, and J. Wu, Strain engineering and one-dimensional organization of metal–insulator domains in single-crystal vanadium dioxide beams, Nat. Nanotech. **4**, 732 (2009).

[25] E. Abreu, M. Liu, J. Lu, K. G. West, S. Kittiwatanakul, W. Yin, S. A. Wolf, and R. D. Averitt, THz spectroscopy of VO_2 epitaxial films: Controlling the anisotropic properties through strain engineering, New J. Phys. **14**, 083026 (2012).

[26] A. Cavalleri, T. Dekorsy, H. H. W. Chong, J. C. Kieffer, and R. W. Schoenlein, Evidence for a structurally-driven insulator-to-metal transition in VO_2: A view from the ultrafast timescale, Phys. Rev. B **70**, 161102(R) (2004).

[27] D. Wegkamp and J. Stähler, Ultrafast dynamics during the photoinduced phase transition in VO_2, Prog. Surf. Sci. **90**, 464 (2015).

[28] M. A. Huber, M. Plank, M. Eisele, R. E. Marvel, F. Sandner, T. Korn, C. Schüller, R. F. Haglund, Jr., R. Huber, and T. L. Cocker, Ultrafast mid-infrared nanoscopy of strained vanadium dioxide nanobeams, Nano Lett. **16**, 1421 (2016).

[29] W.-P. Hsieh, M. Trigo, D. A. Reis, G. A. Artioli, L. Malavasi, and W. L. Mao, Evidence for photo-induced monoclinic metallic VO_2 under high pressure, Appl. Phys. Lett. **104**, 021917 (2014).

[30] J. M. Braun, H. Schneider, M. Helm, R. Mirek, L. A. Boatner, R. E. Marvel, R. F. Haglund, and A. Pashkin, Ultrafast carrier dynamics in VO_2 across the pressure-induced insulator-to-metal transition, New J. Phys. **20**, 083003 (2018).

[31] S. Lysenko, V. Vikhnin, F. Fernandez, A. Rua, and H. Liu, Photoinduced insulator-to-metal phase transition in VO_2 crystalline films and model of dielectric susceptibility, Phys. Rev. B **75**, 075109 (2007).

[32] S. Pauli, R. Herger, P. Willmott, E. Donev, J. Suh, and R. Haglund, X-ray diffraction studies of the growth

of vanadium dioxide nanoparticles, J. Appl. Phys. **102**, 073527 (2007).

[33] Y. Zhao, J. H. Lee, Y. Zhu, M. Nazari, Ch. Chen, H. Wang, A. Bernussi, M. Holtz, and Zh. Fan, Structural, electrical, and terahertz transmission properties of VO_2 thin films grown on c-, r-, and m-plane sapphire substrates, J. Appl. Phys. **111**, 053533 (2012).

[34] R. Lopez, L. C. Feldman, and R. F. Haglund, Jr., Size-Dependent Optical Properties of VO_2 Nanoparticle Arrays, Phys. Rev. Lett. **93**, 177403 (2004).

[35] J. Y. Suh, R. Lopez, L. C. Feldman, and R. F. Haglund, Jr., Semiconductor to metal phase transition in the nucleation and growth of VO_2 nanoparticles and thin films, J. Appl. Phys. **96**, 1209 (2004).

[36] C. Thomsen, H. T. Grahn, H. J. Maris, and J. Tauc, Surface generation and detection of phonons by picosecond light pulses, Phys. Rev. B **34**, 4129 (1986).

[37] See Supplemental material at http://link.aps.org/supplemental/10.1103/PhysRevApplied.11.014054 for details on calculations of strain pulse and elasto-optical response, subtraction of photoelastic contribution from the experimental curves, the experimental setup, and for results at temperatures above the phase transition.

[38] A. Pashkin, C. Kübler, H. Ehrke, R. Lopez, A. Halabica, R. F. Haglund, R. Huber, and A. Leitenstorfer, Ultrafast insulator-metal phase transition in VO_2 studied by multiterahertz spectroscopy, Phys. Rev. B **83**, 195120 (2011).

[39] T. L. Cocker, L. V. Titova, S. Fourmaux, G. Holloway, H.-C. Bandulet, D. Brassard, J.-C. Kieffer, M. A. E. Khakani, and F. A. Hegmann, Phase diagram of the ultrafast photo-induced insulator-metal transition in vanadium dioxide, Phys. Rev. B **85**, 155120 (2012).

[40] V. R. Morrison, R. P. Chatelain, K. L. Tiwari, A. Hendaoui, A. Bruhacs, M. Chaker, and B. J. Siwick, A photoinduced metal-like phase of monoclinic VO_2 revealed by ultrafast electron diffraction, Science **346**, 445 (2014).

[41] B. T. O'Callahan, A. C. Jones, J. H. Park, D. H. Cobden, J. M. Atkin, and M. B. Raschke, Inhomogeneity of the ultrafast insulator-to-metal transition dynamics of VO_2, Nat. Commun. **6**, 6849 (2015).

[42] S. Lysenko, N. Kumar, A. Rua, J. Figueroa, J. Lu, and F. Fernandez, Ultrafast structural dynamics of VO_2, Phys. Rev. B **96**, 075128 (2017).

[43] S. Wall, L. Foglia, D. Wegkamp, K. Appavoo, J. Nag, R. F. Haglund, Jr., J. Stähler, and M. Wolf, Tracking the evolution of electronic and structural properties of VO_2 during the ultrafast photo-induced insulator-metal transition, Phys. Rev. B **87**, 115126 (2013).

[44] P. J. S. van Capel, E. Péronne, and J. I. Dijkhuis, Nonlinear ultrafast acoustics at the nano scale, Ultrasonics **56**, 36 (2015).

[45] H. W. Verleur, A. S. Barker, Jr., and C. N. Berglund, Optical Properties of VO_2 between 0.25 and 5 eV, Phys. Rev. **172**, 788 (1968).

[46] P. Baum, D.-S. Yang, and A. H. Zewail, 4D visualization of transitional structures in phase transformations by electron diffraction, Science **318**, 788 (2007).

[47] S. Lysenko, A. Rúa, V. Vikhnin, F. Fernández, and H. Liu, Insulator-to-metal phase transition and recovery processes in VO_2 thin films after femtosecond laser excitation, Phys. Rev. B **76**, 035104 (2007).

[48] E. Abreu, S. N. Gilbert Corder, S. J. Yun, S. Wang, J. G. Ramírez, K. West, J. Zang, S. Kittiwatanakul, I. K. Schuller, J. Lu et al., Ultrafast electron-lattice coupling dynamics in VO$_2$ and V$_2$O$_3$ thin films, Phys. Rev. B **96**, 094309 (2017).

[49] A. Tselev, E. Strelcov, I. A. Luk'yanchuk, J. D. Budai, J. Z. Tischler, I. N. Ivanov, K. Jones, R. Proksch, S. V. Kalinin, and A. Kolmakov, Interplay between ferroelastic and metal-insulator phase transitions in strained quasi-two-dimensional VO$_2$ nanoplatelets, Nano Lett. **10**, 2003 (2010).

[50] A. Tselev, I. A. Luk'yanchuk, I. N. Ivanov, J. D. Budai, J. Z. Tischler, E. Strelcov, A. Kolmakov, and S. V. Kalinin, Symmetry relationship and strain-induced transitions between insulating M1 and M2 and metallic R phases of vanadium dioxide, Nano Lett. **10**, 4409 (2010).

[51] L. Landau and E. Lifshitz, *Statistical Physics, Part 1* (Pergamon Press, Oxford, 1980).

[52] S. A. Dönges, O. Khatib, B. T. O'Callahan, J. M. Atkin, J. H. Park, D. Cobden, and M. B. Raschke, Ultrafast nanoimaging of the photoinduced phase transition dynamics in VO$_2$, Nano Lett. **16**, 3029 (2016).

[53] B. A. Strukov and A. P. Levanyuk, *Ferroelectric Phenomena in Crystals: Physical Foundations* (Springer, Berlin/Heidelberg, 1998).

[54] H. Sakuma, M. Tomoda, P. H. Otsuka, O. Matsuda, O. B. Wright, T. Fukui, K. Tomioka, and I. A. Veres, Vibrational modes of GaAs hexagonal nanopillar arrays studied with ultrashort optical pulses, Appl. Phys. Lett. **100**, 131902 (2012).

[55] T. Czerniuk, J. Tepper, A. V. Akimov, S. Unsleber, C. Schneider, M. Kamp, S. Höfling, D. R. Yakovlev, and M. Bayer, Impact of nanomechanical resonances on lasing from electrically pumped quantum dot micropillars, Appl. Phys. Lett. **106**, 041103 (2015).

[56] A. Bojahr, D. Schick, L. Maerten, M. Herzog, I. Vrejoiu, C. K. Schmising, C. Milne, S. L. Johnson, and M. Bargheer, Comparing the oscillation phase in optical pump-probe spectra to ultrafast x-ray diffraction in the metal-dielectric SrRuO$_3$/SrTiO$_3$ superlattice, Phys. Rev. B **85**, 224302 (2012).

[57] P. van Capel, D. Turchinovich, H. Porte, S. Lahmann, U. Rossow, A. Hangleiter, and J. Dijkhuis, Correlated terahertz acoustic and electromagnetic emission in dynamically screened InGaN/GaN quantum wells, Phys. Rev. B **84**, 085317 (2011).

[58] M. A. Kats, R. Blanchard, P. Genevet, Zh. Yang, M. M. Qazilbash, D. N. Basov, Sh. Ramanathan, and F. Capasso, Thermal tuning of mid-infrared plasmonic antenna arrays using a phase change material, Opt. Lett. **38**, 368 (2013).

[59] J. D. Ryckman, K. A. Hallman, R. E. Marvel, R. F. Haglund, Jr., and Sh. M. Weiss, Ultra-compact silicon photonic devices reconfigured by an optically induced semiconductor-to-metal transition, Opt. Exp. **21**, 10753 (2013).

[60] R. F. Haglund, Jr., Sh. M. Weiss, and K. Appavoo, Photonic and plasmonic modulators based on optical switching in VO$_2$, Proc. SPIE 9370, 93701C-10 (2015).

[61] O. L. Muskens, L. Bergamini, Yu. Wang, J. M. Gaskell, N. Zabala, C. H. de Groot, D. W. Sheel, and J. Aizpurua, Antenna-assisted picosecond control of nanoscale phase transition in vanadium dioxide, Light: Sci. Appl. **5**, e16173 (2016).

[62] A. Crut, P. Maioli, N. Del Fatti, and F. Vallée, Acoustic vibrations of metal nano-objects: Time-domain investigations, Phys. Rep. **549**, 1 (2015).

[63] A. V. Kimel, A. Kirilyuk, A. Tsvetkov, R. V. Pisarev, and Th. Rasing, Laser-induced ultrafast spin reorientation in the antiferromagnet TmFeO$_3$, Nature **429**, 850 (2004).

[64] G. Ju, J. Hohlfeld, B. Bergman, R. J. M. van de Veerdonk, O. N. Mryasov, J.-Y. Kim, X. Wu, D. Weller, and B. Koopmans, Ultrafast Generation of Ferromagnetic Order via a Laser-Induced Phase Transformation in FeRh Thin Films, Phys. Rev. Lett. **93**, 197403 (2004).

[65] J. A. de Jong, I. Razdolski, A. M. Kalashnikova, R. V. Pisarev, A. M. Balbashov, A. Kirilyuk, Th. Rasing, and A. V. Kimel, Coherent Control of the Route of an Ultrafast Magnetic Phase Transition via Low-Amplitude Spin Precession, Phys. Rev. Lett. **108**, 157601 (2012).

[66] S. L. Johnson, R. A. de Souza, U. Staub, P. Beaud, E. Möhr-Vorobeva, G. Ingold, A. Caviezel, V. Scagnoli, W. F. Schlotter, J. J. Turner et al., Femtosecond dynamics of the collinear-to-spiral antiferromagnetic phase transition in CuO, Phys. Rev. Lett. **108**, 037203 (2012).